Solution Processed PCBM-$CH_3NH_3PbI_3$ Heterojunction Photodetectors with Enhanced Performance and Stability

Yafei Wang[a], Ting Zhang[a], Peng Zhang[a], Detao Liu[a], Long Ji[a], Hao Chen[a], Zhi David Chen[a,c], Jiang Wu[a,b*] , and Shibin Li[a*]

[a] State Key Laboratory of Electronic Thin Films and Integrated Devices, and School of Optoelectronic Information, University of Electronic Science and Technology of China (UESTC), Chengdu, Sichuan 610054, China

[b] Department of Electronic and Electrical Engineering, University College London, Torrington Place, London WC1E7JE, United Kingdom

[c] Department of Electrical & Computer Engineering, and Center for Nanoscale Science & Engineering, University of Kentucky, Lexington, Kentucky 40506, USA

*Corresponding authors: shibinli@uestc.edu.cn, jiang.wu@ucl.ac.uk

Abstract

In this work, an anti-solvent process was used to fabricate a perovskite-PCBM bulk heterojunction, in which PCBM diffused in $CH_3NH_3PbI_3$ and passivated grain boundary defects. Different concentrations of PCBM were studied in this paper. When a low concentration (5mg/ml, 10mg/ml or 15mg/ml) of PCBM was used, the PCBM-$CH_3NH_3PbI_3$ transition layer provided efficient electron collection. With the increase of the concentration of PCBM, a thicker PCBM layer was formed in the bulk heterojunction. Such a thick PCBM resulted in rough perovskite morphology and low photo-carrier collection efficiency. SEM images and metallographic microscope images confirmed that the PCBM upper layer gradually covered grain boundaries of perovskite films with the increase of the PCBM concentration. On the other hand, low concentrations of PCBM improved the light absorption and crystallinity of $CH_3NH_3PbI_3$ films. The PCBM/perovskite heterojunction exhibited a high UV

responsivity of 0.18 AW^{-1} and a response time less than 123ms. This research provides a way to improve the quality of perovskite films and the performance of perovskite photodetectors.

Introduction

Photodetectors are widely applied in imaging, environmental monitoring and optical communications.[1-6] Over the past years, organic-inorganic halide perovskite materials have emerged as one of the most promising materials for optoelectronic devices, particularly photovoltaic cells.[7-13] Recently, increasingly more efforts have been directed to the applications of perovskite materials to photodetectors, phototransistors and so on.[1-2, 14-15]

Most perovskite photodetectors currently are made of a perovskite based heterojunction structure. For example, Lu et al. fabricated a photodetector based on a hybrid bilayer WSe_2-$CH_3NH_3PbI_3$ heterojunction . [1] They found Se vacancies in the WSe_2 monolayer form deep gap levels that act as severe trap states for photo-generated electrons. Improved performance was realized by modification of the WSe_2 monolayer and perovskite functionalization. Zeng's group combined CNTs and $CsPbBr_3$ to make a flexible photodetector. [2] Carbon nanotubes greatly enhanced the conductivity of $CsPbBr_3$ films and the $CsPbBr_3$/CNTs composite film provided efficient carrier transfer. Wu et al. fabricated high performance photoconductors based on $CH_3NH_3PbI_3$ and 2D WS_2. [6] The WS_2 sheet had a high mobility and could efficiently separate charge carriers. From these efforts, it has been shown that charge transfer plays a key role in the performance of perovskite photodetectors. Therefore,

interface engineering is critical for the high performance of perovskite photodetectors. [1-2, 5-6, 13, 16-22]

Herein, we fabricated a $CH_3NH_3PbI_3$/PCBM bulk heterojunction by an anti-solvent process and used it to make high-performance photodetectors. PCBM has been widely employed in inverted perovskite solar cells and $CH_3NH_3PbI_3$/PCBM heterostructure is generally used even though fabrication of a high quality interface has been non-trivial. [23-24] PCBM here also inserted into the grain boundaries. A simple FTO/$CH_3NH_3PbI_3$/PCBM heterostructure patterned with interdigital electrodes (ten channels, length: 1000μm, width: 60μm) was used in this study. The photoresponse of the $CH_3NH_3PbI_3$/PCBM heterojunction device was four orders of magnitude higher than that of a $CH_3NH_3PbI_3$ reference device. The study revealed that PCBM could promote the transfer of carriers. PCBM/perovskite photodetectors exhibited a UV responsivity of 0.18 AW^{-1} and a response time of less than 123ms under a bias of 0.6 V. Without packaging, the device can maintain the performance with minor degradation in the air (23-26°C, 40%-60% relative humidity) for more than 48 hours.

Results and Discussion

The $CH_3NH_3PbI_3$/PCBM bulk heterojunction was fabricated by an anti-solvent process as shown in Figure 1. Different amounts of PCBM were added to chlorobenzene (CB). When the anti-solvent was dripped on a substrate, the PCBM chlorobenzene solution deposited on the perovskite film led to the formation of a PCBM/perovskite heterojunction. PCBM inserted into the grain boundaries of

perovskite films. The PCBM deposited at $CH_3NH_3PbI_3$ grain boundaries, which formed a composite film. The FTO glass was etched into designed patterns as contacts. After washing the film with anti-solvent, the sample was annealed at 100°C for 15 min. In this investigation, five concentrations of PCBM: 5mg/ml, 10mg/ml, 15mg/ml, 20mg/ml and 30ml/ml were studied. PCBM was found to significantly affect the surface morphology and the crystallization of $CH_3NH_3PbI_3$ films. This is explained by the fact that PCBM can separate the notoriously unstable intermediate products from the sensitive polar solvent vapor environment during the spin-coating. [13]

Figure 2 shows the surface metallographic microscope images of perovskite films treated by PCBM chlorobenzene solutions with different concentrations (0mg/ml, 5mg/ml, 10mg/ml, 15mg/ml, 20mg/ml and 30mg/ml). A uniform surface of a perovskite film was obtained when pure CB, 5mg/ml, or 10mg/ml PCBM chlorobenzene solutions were used. As the concentration of PCBM was low, PCBM only slightly influenced the surface morphology of perovskite films. Therefore, a very thin PCBM layer was coated on $CH_3NH_3PbI_3$ to form a thin upper layer. When the PCBM chlorobenzene solution with PCBM concentration of 15mg/ml was employed, some dots appeared on the surface. It illustrates that more PCBM covered the perovskite layer. Furthermore, the surface morphology of the film became more uneven with the increase of the concentration of PCBM, as shown in Figure 2e-f. There are a lot of strip-shape crystals on the surface owed to the formation of a thick PCBM upper layer. The colorful image confirmed the uneven surface morphology of PCBM-$CH_3NH_3PbI_3$ films. Therefore, a dilute PCBM chlorobenzene solution led to

uniform films with smooth surface morphology.

In order to investigate the surface morphology and the micro structure further, SEM images are shown in Figure 3. It is clear that big grains and some boundaries were formed with pure CB washing as shown in Figure 3a. In Figure 3b, the boundaries become thinner indicating that PCBM was coated on the grain boundaries and surface of $CH_3NH_3PbI_3$. Furthermore, grain boundaries are not clear in Figure 3c when the film was washed by the solution with a higher PCBM concentration (10mg/ml). The boundaries are gradually disappeared with the PCBM concentration increases as shown in Figure 3d-f. This is caused by the formation of a separated PCBM upper layer on the perovskite film and hence the perovskite/PCBM bulk heterojunction. Therefore, PCBM can modify the grain boundaries of perovskite films and form a thin upper layer when a relatively low concentration of PCBM (5mg/ml, 10mg/ml and 15mg/ml) was used in the PCBM chlorobenzene washing solvent. The photographs of perovskite films and PCBM chlorobenzene solutions are shown in Figure S1. The analysis of the surface morphology of $CH_3NH_3PbI_3$-PCBM composite films confirmed the formation of the bulk heterojunction structure that is shown in the schematic in Figure 1.

The UV-Vis absorption curves shown in Figure 4a indicate all perovskite films have a good absorption of visible light regardless of PCBM surface modification. Every absorption curve has a steep slope at 760nm corresponding to the $CH_3NH_3PbI_3$ bandgap. We also observe the absorption of perovskite from 700nm to 850nm, as shown in Figure 4b. The absorbance of the films at 760nm are very close, which

indicates perovskite films have similar quality and crystallization. The slightly better UV-Vis absorption of perovskite films treated by 5, 10, 15 and 20 mg/ml PCBM solution should be owing to PCBM that separates the intermediate products from the polar solvent vapor environment. Additionally, the baseline of the perovskite film modified with 30mg/ml PCBM is much higher than the rest. The increase of baseline is owing to the diffuse reflection from a rough surface. [27] It proved that a higher concentration of PCBM in the chlorobenzene solution formed a thick PCBM upper layer on the perovskite film and influenced the surface morphology. This result is consistent with the SEM and metallographic microscope images.

Figure 4c shows the X-ray diffraction (XRD) patterns of perovskite films treated by PCBM chlorobenzene solutions of different concentrations. The XRD patterns with peaks at 14.2°, 28.5° and 31.9°, corresponding to the (110), (220) and (310) planes of perovskite, respectively, are observed in the figure. Each perovskite film has the same crystal structure and the peak of perovskite becomes higher with the increase of the concentration of PCBM in the anti-solvent. Such an enhancement of the XRD intensity indicates a better crystallization or larger average crystal grain size. Therefore, XRD measurements suggest again that PCBM addition in the anti-solvent is very beneficial to the crystal quality of perovskite films. These effects may be explained by the hydrophobicity ability of PCBM which could effectively reduce the interaction between polar solvent vapors and the perovskite nuclei. Through calculating and fitting, we obtained the full width at half maximum (FWHM) of the (110) diffraction peak. The FWHM of the (110) peak for each $CH_3NH_3PbI_3$ film

prepared with different anti-solvents (pure CB, 5, 10, 15, 20 and 30 mg/ml PCBM CB solution) is 0.289°, 0.285°, 0.196°, 0.213°, 0.239° and 0.220°, respectively. The FWHM of the film treated by 10mg/ml (0.196°) or 15mg/ml (0.213°) is obvious lower than that (0.289°) of the sample with pure CB washing. We showed the strength of (110) peaks of $CH_3NH_3PbI_3$ treated by different concentrations of PCBM solutions in Figure 4d. With the increase of PCBM concertation, the crystallization of $CH_3NH_3PbI_3$ was gradually improved. This result is consistent with our previous discussion.

Steady photoluminescence (PL) is carried out to investigate the optical transition properties of the films. The PL spectra are shown in Figure 4e. All the spectra have a similar spectral line shape and peak position. It is obvious that samples prepared with higher PCBM concentrations have a higher steady PL intensity. The intensity of steady PL is associated with both radiative recombination rate and charge transfer rate at the interface. Given the very similar interfaces, the higher steady PL intensity means lower nonradiative recombination.[27-28] This indicates that PCBM effectively improved perovskite film quality and reduced defects and trap sites in perovskite films. We have proposed that PCBM could insert into boundaries of perovskite grains as shown in Figure 1 and Figure 3. The coated PCBM layer became a transport channel for electrons and well passivated the defects at grain boundaries of $CH_3NH_3PbI_3$. PCBM is a widely used n-type electron transport material (ETM) in solar cells. The PL emission of perovskite could be efficiently quenched when the ETM or hole transport material (HTM) was present in solar cell structure. However,

in our study, we have a different device structure (as shown in Figure 1) and PCBM inserts into perovskite crystals. Previous SEM images demonstrated PCBM inserted at grain boundaries was very thin so that this PCBM layer could facilitate transfer of electrons from one perovskite domain to another. The improvement of the crystallization and the quality (morphology, structure, optical absorption etc.) of perovskite films also influenced steady PL measurement. Additionally, a thin inserted PCBM layer could provide a better transport path for electrons. However, the upper PCBM layer does not seem to be important in the carrier transport process. Figure 4f shows the integrated PL intensity of perovskite films via different PCBM CB solution washing. We found the PCBM effectively reduced the nonradiative recombination. The higher concentration PCBM solution we used, the higher integrated steady PL intensity. Hence, this $CH_3NH_3PbI_3$-PCBM bulk heterojunction effectively improved the carriers transport ability of the active layer.

To examine the performance of photodetectors based on different $CH_3NH_3PbI_3$/PCBM films, Figure 5a shows the I-V curves of each sample under illumination conditions. Firstly, the FTO substrate was patterned into interdigital electrodes (ten channels, length: 1000μm, width: 60μm) which are used to collect photocarriers generated in the perovskite films. The bias voltage ranged from -0.6V to 0.6V. It is obvious that the perovskite film treated by the solvent of 15mg/ml PCBM exhibits the highest photocurrent of 67μA at an applied voltage of 0.6V. When $CH_3NH_3PbI_3$ was washing by solvents with 5mg/ml, 10mg/ml and 15mg/ml PCBM concentrations, the photocurrent increased with increasing the concentration of PCBM.

This result is consistent with our previous structural measurements and analysis. Doping low concentrations of PCBM in the chlorobenzene solution would increase the crystal quality and effectively reduce the recombination in perovskite films. A thin PCBM layer connects $CH_3NH_3PbI_3$ grains and then forms the heterojunction structure which was advantageous for the separation and transport of carries. Additionally, due to the band offset between perovskite and PCBM, an energy barrier is formed at the PCBM/perovskite interface. Using higher concentration PCBM solution, too thicker inserted PCBM layer might be disadvantageous for carrier transport. With PCBM fills the gaps between the perovskite grains, the PCBM not only passivates the interface and grain boundaries but also forms a transport path which improves carrier transport at the grain boundaries. However, with further increase in the concentration of PCBM, the photocurrent was decreased because of the formation of a thicker PCBM insert layer. Too much PCBM caused intermixing of $CH_3NH_3PbI_3$ and PCBM. As a result, interfacial states are generated and potentially introduce additional recombination. A thicker PCBM insert layer trapped too many electrons in PCBM domains and thus was not conducive to the transmission of electrons. The transient photocurrent-time (I-t) curves are shown in Figure 5b. This figure shows that the photocurrents of the devices were stable during repeated on/off cycles. The $CH_3NH_3PbI_3$ device based on 15mg/ml PCBM washing also achieved the best photoresponse. Under 0.6V bias voltage, the detectivities of photodetectors with different solution washing (w/o PCBM, with 5mg/ml, 10mg/ml, 15mg/ml, 20mg/ml and 30mg/ml PCBM CB solution) were 0.0024A/W, 0.0058A/W, 0.0073A/W, 0.011A/W, 0.0050A/W and 0.0043A/W,

respectively. Note that, our measurement completed in the light density of 100mW/cm^2. The dark current lines of photodetectors based on different concentration PCBM solution washing are shown in Figure S3. In Figure S3(a), we found dark currents of each photodetectors were all between 10^{-7}A and 10^{-8}A under the bias voltage of 0.6 V. Figure S3(b) shows dark currents of photodetectors under the bias voltage of 2V, and dark current of each device is around 10^{-7}A. It is obvious that the dark current of photodetector with 15mg/ml PCBM washing is slightly higher than those of photodetectors with CB washing or with 5mg/ml PCBM solution washing.

Figure 6a shows the photocurrent of $CH_3NH_3PbI_3$ with 15mg/ml PCBM washing under different bias voltages. The photocurrent of $CH_3NH_3PbI_3$/PCBM heterojunction increased from 67μA to 1500μA under the bias voltage ranged from 0.6V to 10V. At the same time, detectivity of the photodetector increased from 0.0109A/W (bias 0.6V) to 0.273A/W (bias 10V) under white light. When 5V bias voltage was employed, the detectivity of the device was 0.116A/W. Compared with the reference device, the much higher photoresponse illustrated that photocarriers were more efficiently collected in $CH_3NH_3PbI_3$/PCBM bulk heterojunctions. The switching ratio of a photodetector is defined as the photocurrent to dark current ratio (I_{light}/ I_{dark}). Figure 6b shows the I_{light} and I_{dark} of the $CH_3NH_3PbI_3$ detector fabricated with 15mg/ml PCBM washing under the bias voltage of 0.6V. The switching ratio could reach as high as 3×10^3. Both I_{light} and I_{dark} remain almost unchanged over time, suggesting this $CH_3NH_3PbI_3$/PCBM heterojunction has a good stability. At the same time, we also

measured the photoresponse under ultraviolet light of 365nm of the $CH_3NH_3PbI_3$ device prepared by washing with 15mg/ml PCBM. The UV light was 2mW/cm^2. A high photocurrent response of 22μA was achieved. The responsivity of the device for UV light is 0.18A/W. This result illustrates our device has a good response for UV detection.

Furthermore, we tested the stability of reference $CH_3NH_3PbI_3$ and $CH_3NH_3PbI_3$/PCBM photodetectors, as shown in Figure 7a. After 48 hours, $CH_3NH_3PbI_3$/PCBM heterojunction kept 66% photocurrent of the initial value (in air, 23-26°C, 40%-60% relative humidity, in dark). For the $CH_3NH_3PbI_3$ reference photodetector, the photocurrent decreased from 14μA to 3μA, 14 times lower than that of the $CH_3NH_3PbI_3$/PCBM device. The photocurrent of the reference device after 48 hours only remained 21% compared the initial state. Such improved stability of the heterojunction device should be owing to the better crystallization and morphology of perovskite films. Meanwhile, PCBM upper layer also prevented the perovskite contact with oxygen or water because of its hydrophobicity.[25-26] After 48h, the photoresponse for UV light was also measured, as shown in Figure S2. $CH_3NH_3PbI_3$/PCBM heterojunction showed a good UV stability consistent with measurements under the white light source. A Keithley 4200 semiconductor parameter analyzer was used to measure the response time. The rise time and fall time are defined as the current transition time from the minimum to the maximum current and from maximum to minimum, respectively. Figure 7b shows the rise time is less than 123ms and the fall time is less than 180ms. The photoresponse can be even faster than

this when a high-resolution scan mode is used. Such a high response time also suggested a low density of trap states at the perovskite boundaries.

Conclusion

A facile solution process has been used for preparing $CH_3NH_3PbI_3$/PCBM bulk heterojunction photodetectors on patterned FTO. We found addition of PCBM in the antisolvent solution could effectively improve the quality of $CH_3NH_3PbI_3$ films and lead to better optical properties, morphology and crystallization. The insert PCBM layer also well passivated the defects at grain boundaries of $CH_3NH_3PbI_3$ domains. By using 15mg/ml PCBM in the antisolvent solution, we achieved the best photoresponse of 67μA that was 4 times higher than that of the $CH_3NH_3PbI_3$ device under 0.6V bias. Compared with $CH_3NH_3PbI_3$ reference photodetectors, $CH_3NH_3PbI_3$/PCBM heterojunction photodetectors were more stable, and after 48 hours, the performance remained 66%, whereas, only 21% for the reference device. Overall, this work may supply a new and simple way for the solution engineering of perovskite composite materials toward stable and high-performance perovskite photodetectors.

Experiment Section

Materials. PbI_2, CH_3NH_3I, and PCBM were purchased from YouXuan. Solvents, such as 2-Propanol (IPA, 99. 5%), DMF, DMSO, and acetone, were provided by Dyesol and YouXuan.

Device Fabrication. Firstly, interdigital electrodes was etched on FTO glass substrate by using laser. The spacing between two neighboring fingers was controlled to be 60μm. The whole effective area of each device was about 0.06cm^2. Secondly, we

deposited $CH_3NH_3PbI_3$ film on this patterned FTO substrate. When we measured the performance of photodetectors, the bias voltage was applied across interdigital electrodes. The detailed fabrication process was described as follow. The etched FTO glass substrates were cleaned sequentially in alkaline detergent, acetone, ethanol, and DI water for 15 minutes each, followed by drying with N_2 flow. $CH_3NH_3PbI_3$ was synthesized using the one-step spin coating method and the experiment was carried out in a glove box in nitrogen ambient. The perovskite solution contains 461 mg PbI_2, 231 mg MAI in 0.6 ml DMF, and 0.07 ml DMSO. 80μl perovskite solution was spin-coated at 4000 rpm for 25s. The chlorobenzene and PCBM chlorobenzene solution (5mg/ml, 10mg/ml, 15mg/ml, 20mg/ml and 30mg/ml) were respectively poured on the samples in the first 5 seconds. In order to prevent PCBM reunion. PCBM (99.9%, Toronto Research Chemicals) dissolved in chlorobenzene (99.9%, YouXuan). This solution was vigorously stirred for 2 hours and sonicated for 2 hours. Then the PCBM CB solution stirred for a further hour. The volume of anti-solvent solution was more than 200μl. The samples were annealed at 60 °C for 1 min and then 100 °C for 10 min.

Measurement and Characterization

X-ray diffraction (XRD) measurements were carried out using a Bede D1 system with Cu Kα radiation. Scanning electron microscope (SEM) images were obtained using field emission fitting SEM (FEI-Inspect F50, Holland). The UV-vis absorption spectra were measured by an ultraviolet-visible (UV–vis) spectrophotometer (Schimadzu UV-3101 PC). Current-voltage measurements were carried out using a

Keithley 2400 under different illumination from a solar simulator (Newport Oriel Solar, 64023A). The sun light was calibrated using a standard Si-solar cell (Oriel, VLSI standards) and a photometer. Metallographic microscope images were carried out by MZ5000 (Jiangnan Yongxin). Steady PL curves were measured by F-4600 Fluorescence Spectrophotometer (HITACHI).

Acknowledgement

This work was supported by the National Natural Science Foundation of China under grant nos. 61574029, 61421002, 61574029, and 61371046. This work was also partially supported by University of Kentucky.

Reference

[1] J. Lu, A. Carvalho, H. Liu, S.X. Lim, A.H. Castro Neto, C.H. Sow, Angewandte Chemie, 128 (2016) 12124-12128.

[2] X. Li, D. Yu, J. Chen, Y. Wang, F. Cao, Y. Wei, Y. Wu, L. Wang, Y. Zhu, Z. Sun, J. Ji, Y. Shen, H. Sun, H. Zeng, ACS Nano, 11 (2017) 2015-2023.

[3] H. Fan, W. Shi, X. Yu, J. Yu, Synthetic Metals, 211 (2016) 161-166.

[4] W. Wang, D. Zhao, F. Zhang, L. Li, M. Du, C. Wang, Y. Yu, Q. Huang, M. Zhang, L. Li, J. Miao, Z. Lou, G. Shen, Y. Fang, Y. Yan, Advanced Functional Materials, 27 (2017) 1703953.

[5] S. Tong, J. Sun, C. Wang, Y. Huang, C. Zhang, J. Shen, H. Xie, D. Niu, S. Xiao, Y. Yuan, J. He, J. Yang, Y. Gao, Advanced Electronic Materials, 3 (2017) 1700058.

[6] C. Ma, Y. Shi, W. Hu, M.H. Chiu, Z. Liu, A. Bera, F. Li, H. Wang, L.J. Li, T. Wu, Adv Mater, 28 (2016) 3683-3689.

[7] X. Yin, Z. Xu, Y. Guo, P. Xu, M. He, ACS Appl Mater Interfaces, 8 (2016) 29580-29587.

[8] S. Li, P. Zhang, H. Chen, Y. Wang, D. Liu, J. Wu, H. Sarvari, Z.D. Chen, Journal of Power Sources, 342 (2017) 990-997.

[9] F. Dong, Y. Guo, P. Xu, X. Yin, Y. Li, M. He, Science China Materials, 60 (2017) 295-303.

[10] X. Yin, Y. Guo, Z. Xue, P. Xu, M. He, B. Liu, Nano Research, 8 (2015) 1997-2003.

[11] S. Li, P. Zhang, Y. Wang, H. Sarvari, D. Liu, J. Wu, Y. Yang, Z. Wang, Z.D. Chen, Nano Research, 10 (2016) 1092-1103.

[12] D. Zhao, C. Wang, Z. Song, Y. Yu, C. Chen, X. Zhao, K. Zhu, Y. Yan, ACS Energy Letters, (2018) 305-306.

[13] Y. Wu, X. Yang, W. Chen, Y. Yue, M. Cai, F. Xie, E. Bi, A. Islam, L. Han, Nature Energy, 1 (2016) 16148.

[14] A.R. Yusoff, H.P. Kim, X. Li, J. Kim, J. Jang, M.K. Nazeeruddin, Adv Mater, 29 (2017).

[15] D. Li, H.C. Cheng, Y. Wang, Z. Zhao, G. Wang, H. Wu, Q. He, Y. Huang, X. Duan, Adv Mater, 29 (2017).

[16] L. Shen, Y. Fang, D. Wang, Y. Bai, Y. Deng, M. Wang, Y. Lu, J. Huang, Adv Mater, 28 (2016) 10794-10800.

[17] P. Li, B.N. Shivananju, Y. Zhang, S. Li, Q. Bao, Journal of Physics D: Applied Physics, 50 (2017) 094002.

[18] W. Wang, Y. Ma, L. Qi, Advanced Functional Materials, 27 (2017) 1603653.

[19] D. Zhao, Y. Yu, C. Wang, W. Liao, N. Shrestha, C.R. Grice, A.J. Cimaroli, L. Guan, R.J. Ellingson, K. Zhu, X. Zhao, R.-G. Xiong, Y. Yan, Nature Energy, 2 (2017) 17018.

[20] J. Ding, S. Du, Y. Zhao, X. Zhang, Z. Zuo, H. Cui, X. Zhan, Y. Gu, H. Sun, Journal of Materials Science, 52 (2016) 276-284.

[21] Y. Wang, R. Fullon, M. Acerce, C.E. Petoukhoff, J. Yang, C. Chen, S. Du, S.K. Lai, S.P. Lau, D. Voiry, D. O'Carroll, G. Gupta, A.D. Mohite, S. Zhang, H. Zhou, M. Chhowalla, Adv Mater, 29 (2017).

[22] J. Zhou, Y. Chu, J. Huang, ACS Appl Mater Interfaces, 8 (2016) 25660-25666.

[23] S. Yin, K. Gao, S. Xie, A. Saxena, Organic Electronics, 53 (2018) 96-100.

[24] J. Wang, X. Xiang, X. Yao, W.-J. Xiao, J. Lin, W.-S. Li, Organic Electronics, 39 (2016) 1-9.

[25] K. Huang, C. Wang, C. Zhang, S. Tong, H. Li, B. Liu, Y. Gao, Y. Dong, Y. Gao, Y. Peng, J. Yang, Organic Electronics, (2018).

[26] S. Sutthana, K. Hongsith, P. Ruankham, D. Wongratanaphisan, A. Gardchareon, S. Phadungdhitidhada, D. Boonyawan, P. Kumnorkaew, A. Tuantranont, S. Choopun, Current Applied Physics, 17 (2017) 488-494.

[27] Y. Wang, J. Wu, P. Zhang, D. Liu, T. Zhang, L. Ji, X. Gu, Z. David Chen, S. Li, Nano Energy, 39 (2017) 616-625.

[28] P. Zhang, J. Wu, T. Zhang, Y. Wang, D. Liu, H. Chen, L. Ji, C. Liu, W. Ahmad, Z.D. Chen, S. Li, Adv Mater, 30 (2018).

Figure 1

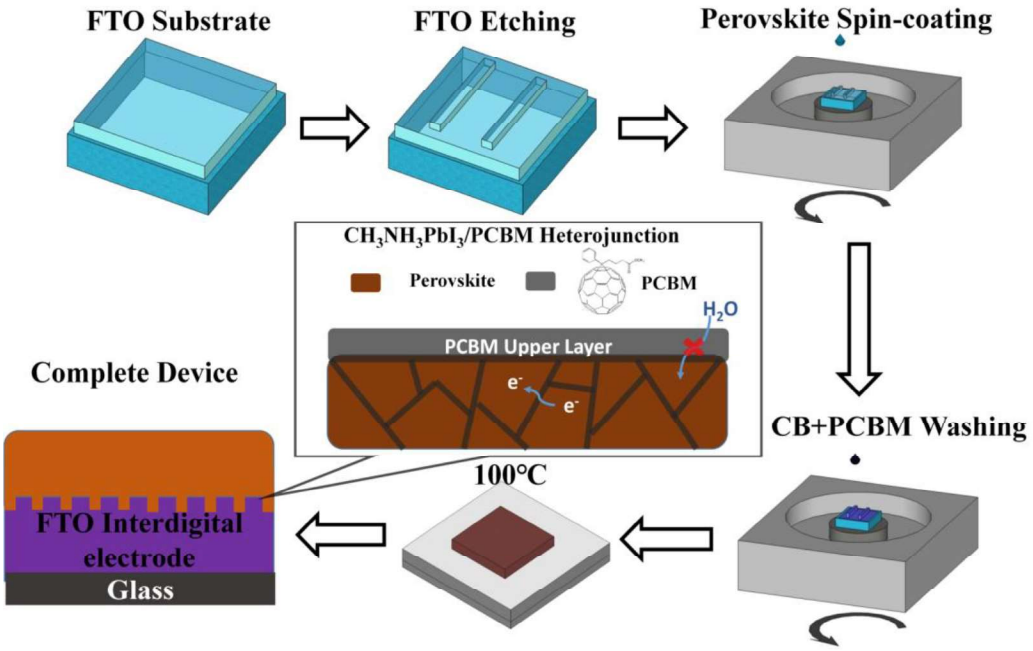

Figure1: The schematic diagram of fabrication methods for photodetectors.

Figure 2

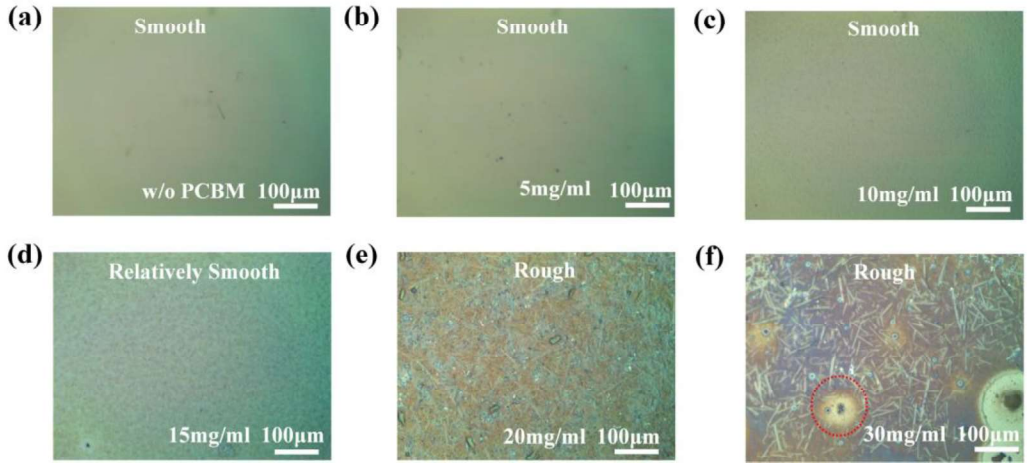

Figure2: (a)-(f) Metallographic microscope images of perovskite films using CB, 5mg/ml PCBM, 10mg/ml PCBM, 15mg/ml PCBM, 20mg/ml PCBM and 30mg/ml PCBM solution washing processes, respectively.

Figure 3

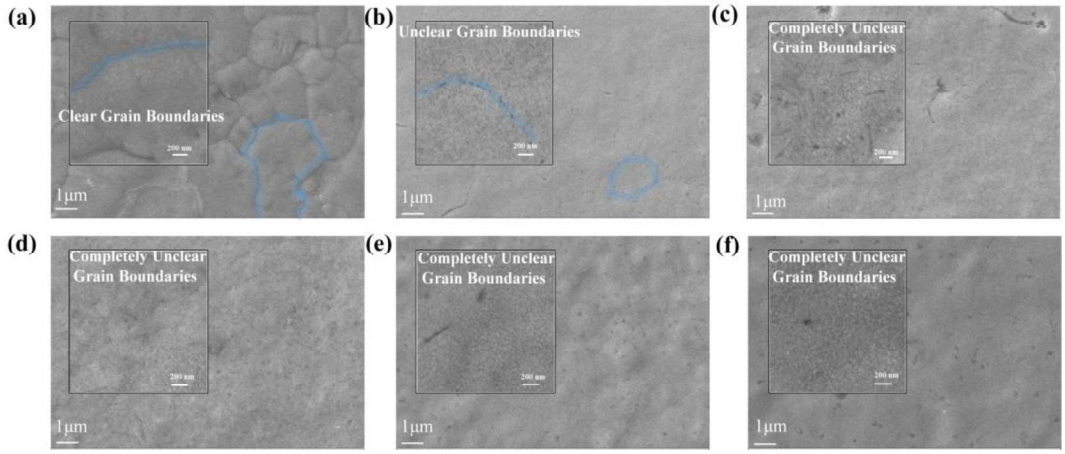

Figure3: (a)-(f) SEM images of perovskite films using CB, 5mg/ml PCBM, 10mg/ml PCBM, 15mg/ml PCBM, 20mg/ml PCBM and 30mg/ml PCBM solution washing processes, respectively.

Figure 4

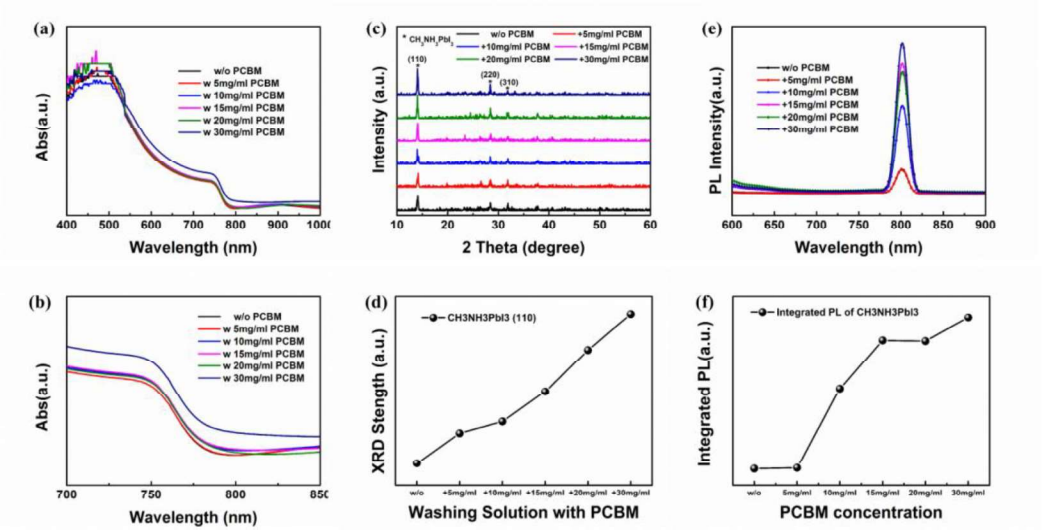

Figure4: (a)-(b) UV-vis absorption spectra (range from 400 nm to 1000 nm), UV-vis absorption spectra (range from 700 nm to 850 nm), (c)-(d) XRD, (110) XRD peak strength, (e)-(f) Steady PL and intergradient PL values of perovskite using different anti-solvents (CB, 5mg/ml PCBM, 10mg/ml PCBM, 15mg/ml PCBM, 20mg/ml PCBM and 30mg/ml PCBM solution) in fabrication

Figure 5

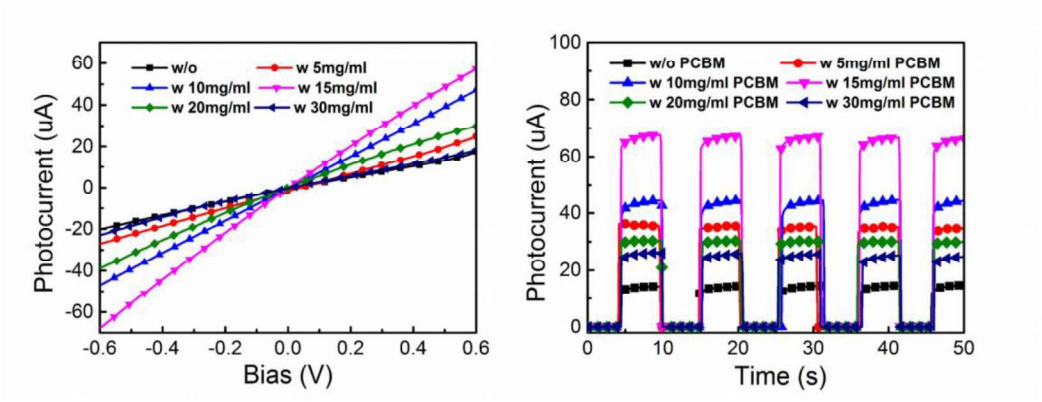

Figure5: (a)-(b) The I-V curves and photocurrent-time (I-t) curves of perovskite films using CB, 5mg/ml PCBM, 10mg/ml PCBM, 15mg/ml PCBM, 20mg/ml PCBM and 30mg/ml PCBM solution washing processes

Figure 6

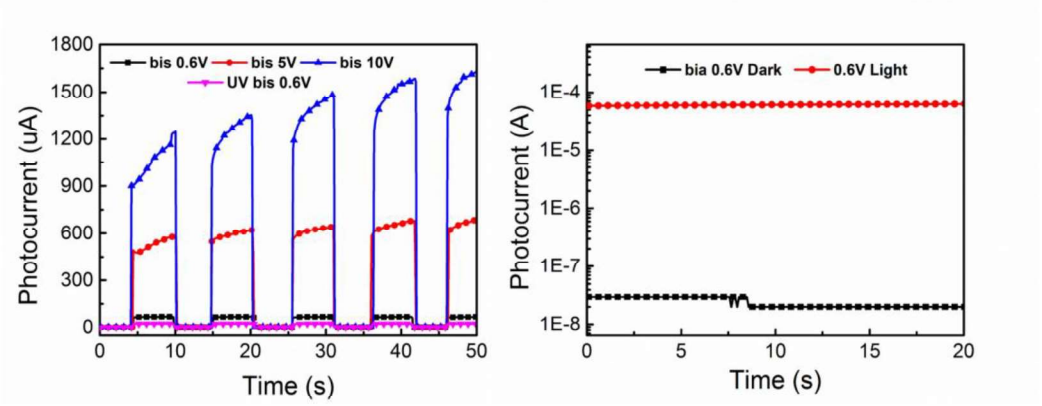

Figure6: (a) The photocurrent of $CH_3NH_3PbI_3$ with 15mg/ml PCBM washing under different bias voltage (0.6V, 5V and 10V). (b) The I_{light} and I_{dark} of $CH_3NH_3PbI_3$ with 15mg/ml PCBM washing under the bias voltage of 0.6V.

Figure 7

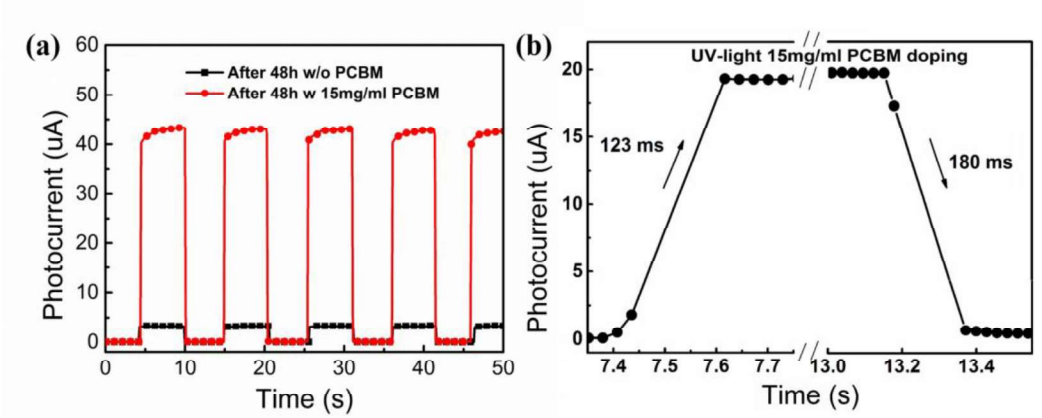

Figure7: (a) The photocurrent-time (I-t) curves of perovskite films using CB and

15mg/ml PCBM solution washing processes after 48 hours of preparation. (b) The rise time and the fall time of perovskite photodetector using 15mg/ml PCBM solution washing under UV light (2mW/cm^2, 365 nm).

Supporting Information

Figure S1 shows the photographs of PCBM solutions and perovskite films obtained using different concentrations of PCBM solution (pure CB, 5mg/ml, 10mg/ml, 15mg/ml, 20mg/ml and 30mg/ml). Figure S2 shows the photoresponse of $CH_3NH_3PbI_3$/PCBM heterojunction based on 15mg/ml PCBM solution washing for UV light after the fabrication of 48h.

Figure S1

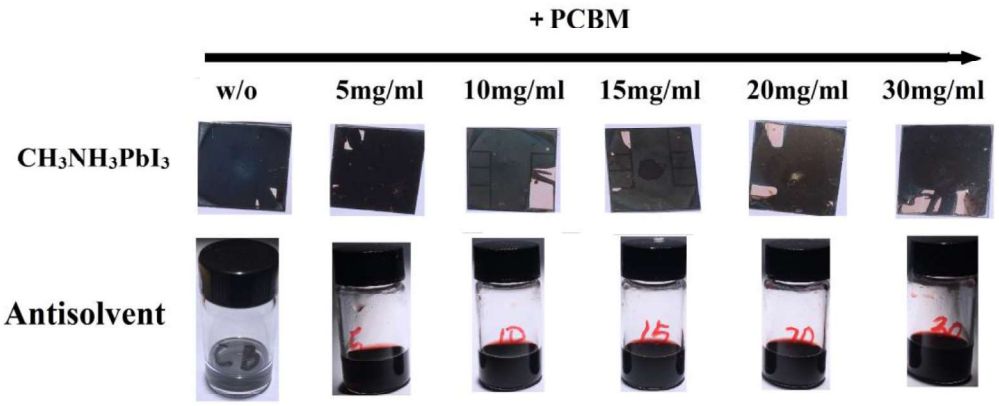

Figure S1: Photos of perovskite films using CB, 5mg/ml PCBM, 10mg/ml PCBM, 15mg/ml PCBM, 20mg/ml PCBM and 30mg/ml PCBM solution as anti-solvent. And photos of PCBM solutions with different concentration.

Figure S2

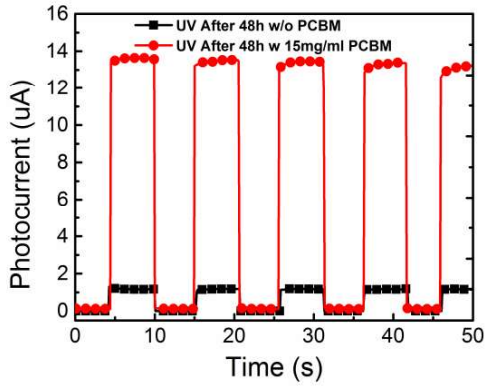

Figure S2: The photocurrent-time (I-t) curves of perovskite films using CB and 15mg/ml PCBM solution washing processes after 48 hours of preparation (under UV light: 365 nm, 2mW/cm^2).

Figure S3

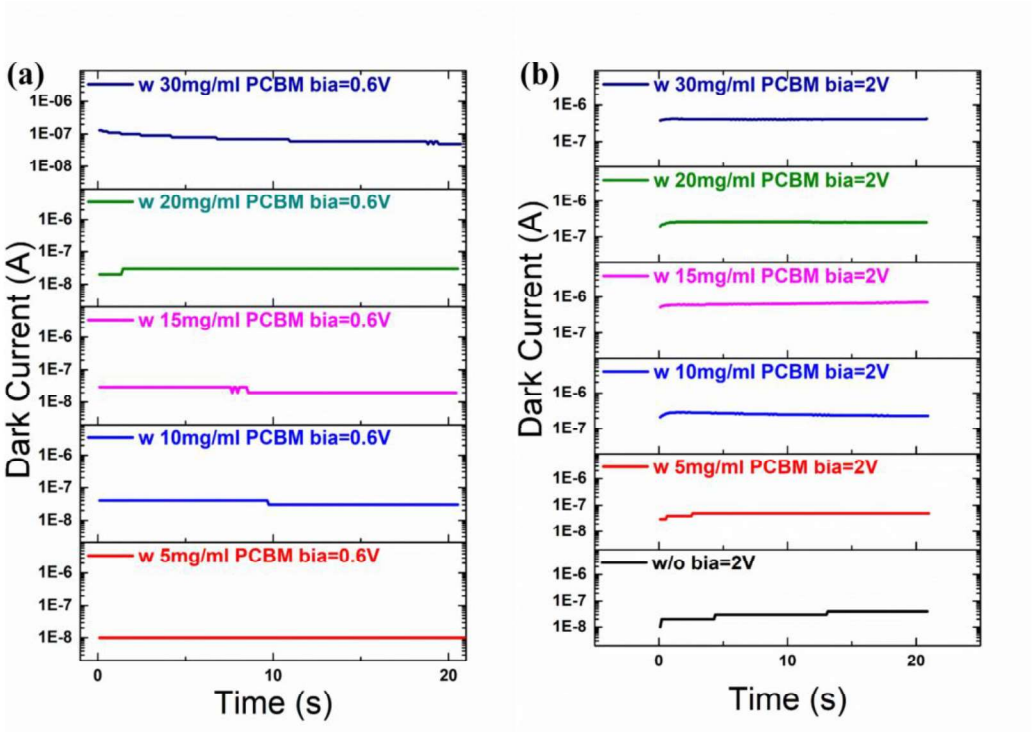

Figure S2: The dark current curves of perovskite films using CB, 5mg/ml PCBM, 10mg/ml PCBM, 15mg/ml PCBM, 20mg/ml PCBM and 30mg/ml PCBM solution as anti-solvent. (a) Bias voltage was 0.6V. (b) Bias voltage was 2V.